COMPUTER-AIDED DETECTION AND SEGMENTATION OF OBJECTS ON MEDICAL IMAGES

Tatjana Belikova
Institute for Information Transmission Problems Russian Academy of Sciences (Moscow Russia)
e-mail: belik@iitp.ru
Roman Palenichka* and Iryna Ivasenko*
* Institute of Physics and Mechanics (Lviv, Ukraine)
e-mail: ivasenko@ah.ipm.lviv.ua

ABSTRACT

Series of methods for improved detecting and segmenting objects, situated on a complex background, have been developed. Model-based detection was applied for automatic detection and segmentation of the objects of interest on initial images and images after optimal filtering. The optimal linear filter was used to improve imaging of the object (its details and margin) on the observed image. Filtering of small-size details to improve false alarm and misdetection rates then followed the segmentation procedure. Developed series of methods were tested on test images and real medical images (lung tomograms) with small solitary nodules. A comparison of segmentation results obtained before and after optimal filtering showed that optimal filtering allows to outline the object region on medical images better and helps to identify more precisely the object margin. The developed series of methods can be useful for computer-assisted detection, segmentation, and analysis of low contrast flaws (lesions) on a complex image background that is important for solving of numerous medical tasks and for technical tasks of material inspection.

1. INTRODUCTION

Automating detection and segmentation of lesions and organs are in the center of interest in many medical problem solutions, starting from actual tasks of image screening, following differential diagnosing, 3-D imaging, surgery, nuclear treatment, and in many others.

Development of Picture Archiving and Communication Systems (PACS) opens new extended possibilities for computer-assisted manipulation, processing, and handling medical images, which could improve the efficacy of medical investigations. Achievements of Computer-Assisted Radiology (CAR) such as multi-modality imaging and multimedia displaying of medical data, digital image processing and computer-aided decision-making [Proc00a] give users new facilities, which surpass their current diagnostic capability.

Further development of computer-assisted radiology is associated with automated image analysis that is to support image analysis and interpretation by an expert. Automatic detection and segmentation of images are very important steps on this way.

Numerous investigators have explored automatic object detection and image segmentation. The contour based method of object detection and feature extraction is often used in different modifications [Breil99]. Petrosian and Wei investigated the contribution of texture features to detection and classification of masses and normal tissue [Petrs94, Wei97]. The wavelet analysis is used in medical image processing for segmentation and detection of diagnostically important object, in particular, microcalcifications [Chen97].

In this paper, we present a robust structural approach to automatic object detection and image segmentation. It is based on a polynomial regression model of images [Palen99a, b]. Robust estimation of model parameters provides easy tuning and fitness to the object. A relevance function used for detection of objects of interest provides fast localization of objects of interest or their parts and feature extraction [Palen00].

The goal of our work is to develop methods for automatic detection and segmentation of low contrast objects located on a complex image background. The other goal is to propose the ways

for better automatic matching segmented region to the object or the region of interest.

We tried facilities of optimal filtering [Belik96] to improve imaging of details, structures and object margin on the observed image. We compared the results of segmentation before and after optimal filtering to test whether such preprocessing could improve matching of automatically segmented and real region of the object.

Thus our sub goals were: 1) to detect the object on the image; 2) to perform image preprocessing by optimal filtering; 3) automatically mark the region with the object on the initial and processed image; 4) to outline margins of segmented areas; 5) to compare the margin of the segmented region with the real object margin or with the margin outlined manually by a physician, 6) to give recommendation for improved detecting and segmenting objects, situated on a complex background.

Developed methods of segmentation are presented in Chapter 2.1. Method of optimal filtering is described in Chapter 2.2. Comparison of segmentation results obtained for the original and processed images is given in Chapter 3. Conclusions and recommendations one can find in Chapter 4.

2. METHODS AND MATERIALS

2.1 Object detection and segmentation

The relevance function [Palen00] is used to localize the region of interest (the region with a nodule on a tomogram). It takes higher values in points belonging to the object of interest than in points of the background. The optimal threshold for image binarization (SEGM1) can be derived by the principle of maximum a posteriori probability and using the model of a two-region image fragment. Having a variable $z(i,j)=g(i,j)-f(i,j)$, the decision about the object's presence or absence for each point (i,j), is made by the inequality:

$$\frac{P(z/object)}{P(z/no-object)} \geq \frac{P(no-object)}{P(object)}, \qquad (1)$$

where *P(object)* and *P(no-object)* are the respective *a priori* probabilities, *P(z/object)* and *P(z/no-object)* are conditional distributions of z. Assuming the underlying image model and Gaussian noise, these values have Gaussian distributions $\mathbf{N}(h, \sigma^2)$ and $\mathbf{N}(0, \sigma^2)$ for the object and no-object, respectively, and the Eq. 1 can be reduced to testing

$$g(i,j) \geq f(i,j) - \frac{h}{2} - \frac{\sigma^2}{h} \cdot \ln\theta(i,j), \qquad (2)$$

where $\theta(i,j)$ is the right part of the Eq. 2; h is the local contrast as a difference value between the object and background intensities. It takes a positive value if the object is brighter than the background, and a negative value is in the opposite case. The ratio of a priori probabilities *P(object)* and *P(no-object)* is different for the object region and the background region: it should be higher in the object's region $O(i,j)$ and lower for the supposed background's region $B(i,j)$. The value of the noise variance σ^2 (polynomial regression residuals) is supposed to be known otherwise it is estimated from the current region of interest [Palen00].

For the segmentation of low-contrast areas possibly belonging to the nodule (parts of the nodule or blood vessels) local contrast h is calculated using structure-adaptive procedure based on the structural image model (SEGM2). It consists of the definition of multiple background structuring regions $\{V_l(i,j)\}$, where $l=1,...,L$ with respect to the background region $B(i,j)$ located at the focus of attention (i,j) and computation of L partial estimates for the local contrast h.

$$h = \max_{1 \leq l \leq L} \left\{ \left| \sum_{(m,n) \in V_l} (g(m,n) - f(m,n)) \right| \right\} \qquad (3)$$

where $f(m,n)$ is the estimated value of the intensity function in point (m,n) based on the polynomial coefficients estimated over the object region $O(i,j)$, $g(m,n)$ is the original image.

For the correction of object shape and noise removal morphological operation of opening (with 90% erosion fitting) was fulfilled after binarization of images (SEGM3). In the experiments the size of the structuring element was equal to 0,5 and 0,75 of the object size.

2.2. Digital image processing

A method for optimal digital filtering [Belik96] has been applied to improve imaging of informative features of the object of interest (small solitary pulmonary nodules on lung tomograms) [Belik94]. There were specific features of the object shape and margins; vascular shadows converging to the nodule, etc. Experiments have been carried out to create an optimal filter for better imaging of diagnostically important structures, which were treated as a useful signal. The fulfilled steps involved: 1) modeling of the mixture of the background and the useful signal for the observing image set; 2) development of the optimal filter to display better informative details by suppressing the impact of the image background; 3) modeling of the background; 4) testing of the processed images by the experts in order to select the background model, which allow the best imaging of diagnostic structures and the highest efficacy of image interpretation by a physician [Belik96]. The feedback was used to find the optimal filter, which met the expert criteria,

and gave the best presentation of the object details and its margin.

The original medical image *X* is regarded as a mixture of the useful signal *U* and the noise *W*, where *U* were diagnostically important details and structures of the nodule and *W* – the reminder part of the image (a total image background). The latter is a combination of a signal from adjacent normal anatomic background structure *B* and from noise *N* of the image registration and image digitizing systems:

$$X=U+W=U+B+N. \quad (4)$$

We developed an optimal filter A, which could emphasize diagnostically important details of the nodule by eliminating a total background influence. The estimation $U' = AX$ has to be found, which is the closest to the useful signal *U* by a specified performance criterion R= ||*U-U'*||=min.

Barrett H.H. and Swindell W. have shown in [Baret96] that medical image data can be well approximated by a Gaussian at count levels typical of clinical imaging. It has been shown for X-ray tomograms, CT images, MR images and some other medical images that every local collection of tissue samples has a Gaussian distribution. Continuum of Gaussians is needed to represent continuum of tissues entire distributions [Aulwd97]. Furthermore, for low-contrast signals the dependence of the noise on the signal is negligible; consequently, the noise is well approximated by a signal-independent Gaussian noise. Object variability, known as "anatomical noise" [Baret96] can be also presented by an arbitrary known (or estimated) covariance; hence, we can assume that the probability density function of initial signal is multivariate normal. Low contrast “anatomical noise” of lung tissue is Gaussian and independent on the remainder of the observing signal.

The filter A was developed with the following assumptions:

1. the registration and input systems give noises that can be described with an additive model;
2. there are no dense objects in the anatomic background tissues that shield the region of interest;
3. the signal of the diagnostically important feature and the signal of total background are independent;
4. diagnostically important feature cannot be modeled, but the background is typical for the analyzed class of images and thus it can be formalized (modeled).

Optimal filters were obtained by using the criterion of a minimal mean square error in estimation of the useful signal:

$$R(U,U') = <(U - AX)^2> = \min, \quad (5)$$

where the averaging <.> was performed over all random values of the signal X.

Several models of background were applied and tested to find the optimal filter which is the best according to the listed expert criteria:

1. processing emphasizes the specific nodule features and makes them more distinct;
2. processing improves efficacy of diagnosis and does not introduce artifacts, which could reduce the diagnostic accuracy;
3. all the structures identified by the processing have analogs in the morphological section (in the histotopogram) [Belik94].

The operator A was chosen in the class of linear operators that allow to use fast algorithms for image processing. The optimal linear filter (Wiener filter) was specified with

$$A=K_U / K_X= (K_X - K_W)/ K_X, \quad (6)$$

where the background *W* is determined by its covariance matrix K_W with the mean $\overline{W}$=0, K_X - covariance matrix of the original image, $K_W^{-1} K_W = I$, *I*- the identity matrix and K_U is the unknown covariance matrix of the useful signal *U*.

As the signal of the diagnostically important feature and the signal of the total background were regarded to be independent, the estimate of K_U was found as the difference of the appropriate covariance matrixes (or of estimates of the power spectra) of the origin image K_X and of the total background K_W.

$$K_U = K_X - (K_B + K_N) = K_X - K_W \quad (7)$$

The total image background was modeled using fragments of original tomograms without a nodule. Several background models W' were constructed to find K_U and to create the optimal filter:

Model 1: The averaged background of T tomograms of the same class;

Model 2: The isotropic part of the tomogram without trend of the video signal (fragments with nearly constant values of the local mean and the standard deviation);

Model 3: The low anisotropy of the tomogram with small video signal trend (fragments with little affected values: up to 10% of the appropriate mean values).

Model 4. The high anisotropy of the tomogram (fragments with higher affected values).

Initial mean values and standard deviations (m_W, σ_W) of these fragments were standardized and chosen equal to those of the tested image background (m_X, σ_X):

$$v'(i,j) = (v'(i,j) - m_W)\sigma_X / \sigma_W + m_X, \quad (8)$$

where $v'(i,j)$ and $v(i,j)$ are standardized and initial pixels of the background sample.

Mean values and standard deviations were then computed and tested in a local area of each point of the background sample. These local areas were rectangular with the size that corresponded to the mean size (1.5 cm) of the nodules.

The estimates $K' = |K'(k,l)|$ of covariance matrixes, K_X and K_W were computed

$$K'(k,l) = \sum_{i=0}^{P-1}\sum_{j=0}^{Q-1} v'(i,j)v'(k-i,l-j)/PQ. \qquad (9)$$

Here $v'(i,j)$ is an element of the appropriate matrix of the original image or of the background model W', $K'(k,l)$ is an element of estimated matrix, *P, Q* - number of lines and rows in this matrix, m- a mean value.

We applied a size-based filtering [Choch88] to remove small-size regions from the segmented image. This procedure was performed to improve false alarm and misdetection rate when segmentation followed optimal linear filtering.

Method for quasi optimal filtering was proposed to realize real-time image processing [Belik96].

3. RESULTS

We tested developed methods in the task of automatic detection and segmentation of solitary pulmonary nodules on lung tomograms. Experiments with test images have been carried out as well.

We modeled lung nodules by a low contrast circle against a constant background. Gaussian blurring with kernel of 10x10 pixels was used on the right part of the circle margin to model unsharpness and invasion of nodule margin into the background We added Gaussian noise of different levels (standard deviation σ=2,…, 20) to this image in order to model a surrounding lung tissues [Baret96] (see Fig. 1a). These initial modeling images were processed by optimal linear filters (7) (Fig. 1b). The initial and processed modeling images were used in test experiments on object detection and segmentation.

All studied cases with pulmonary nodules were discovered by annual screening by means of radiography. Conventional (linear) coronal plane tomograms with 2 mm section thickness were used for experiments with medical images. The slice was centered through the nodule. One or two contiguous sections with 3 mm advance between the slices have been done for some cases as well.

About 20 images with pulmonary nodules up to 3 cm in size were selected for our experiments with lung tomograms. All tomograms had morphologically verified diagnosis. There were nodules with margin of different kind (smooth, angular, spicular, with invasion into surrounding tissues, with converging vessels, sharp and not sharp).

Original linear tomograms were digitized with step of 100 micron (5.0 line pairs per millimeter) to get 1024 x 1024x 8 bits matrix having 256 levels of gray. The use of linear tomograms and such a digitization enabled an acquisition of high spatial resolution of anatomical details that were necessary for the experiment with outlining of lung nodules margin. Original digitized images and images after optimal filtering were used in our experiments (see examples on Fig. 2a-b).

We tested segmentation algorithms, described in Chapter 2.1. on test images. Graphics on Fig. 3 present a comparison of false alarm rate and misdetection rate calculated for SEGM1, SEGM2 and SEGM3 of the initial and processed images and dependent on the standard deviation of Gaussian noise in the segmentation window. False alarm rate was calculated as a probability of detection of the background points as the object points. Misdetection rate was calculated as a probability of detection of the object point as the background points. The region belonging to the object was manually outlined by a physician (see contours on Fig. 1c-d) and used for the false alarm and misdetection rate comparison.

SEGM1. Our experiments with test images showed that this kind of segmentation extracts well the object for both initial and processed test images. Results of such a segmentation of initial test images (Fig. 1a) and processed test image (Fig. 1b) are presented on Fig. 1c-d (white). Our experiments showed that segmentation SEGM1 gave good extraction of the object region for the test images, but in the case of high levels of noise it caused cutting of blurred part of object margin. After segmentation of initial test images the damaged object contours were smoother in comparison with those on the processed test images. The comparison (see Fig. 3) showed, that SEGM1 gave the smallest false alarm rate and the largest misdetection rate for the initial as well as for the processed images.

SEGM2. We tried a two-level segmentation to avoid margin distortions, resulted from the segmentation, SEGM1. The two-level segmentation of the initial and processed test images are presented on Fig, 1 (c-d) (gray). The segmentation SEGM2 extracted the object of interest and preserved a fuzzy part of the object margin. After optimal filtering numerous additional small-size regions have been segmented on the processed images, as optimal filter emphasized manifestation of informative (diagnostically important) details of such a size on the object margin and on the image at whole.

Fig. 3 shows that SEGM2 of the initial and processed images has the highest false alarm rate and the smallest misdetection rate. False alarm rates of

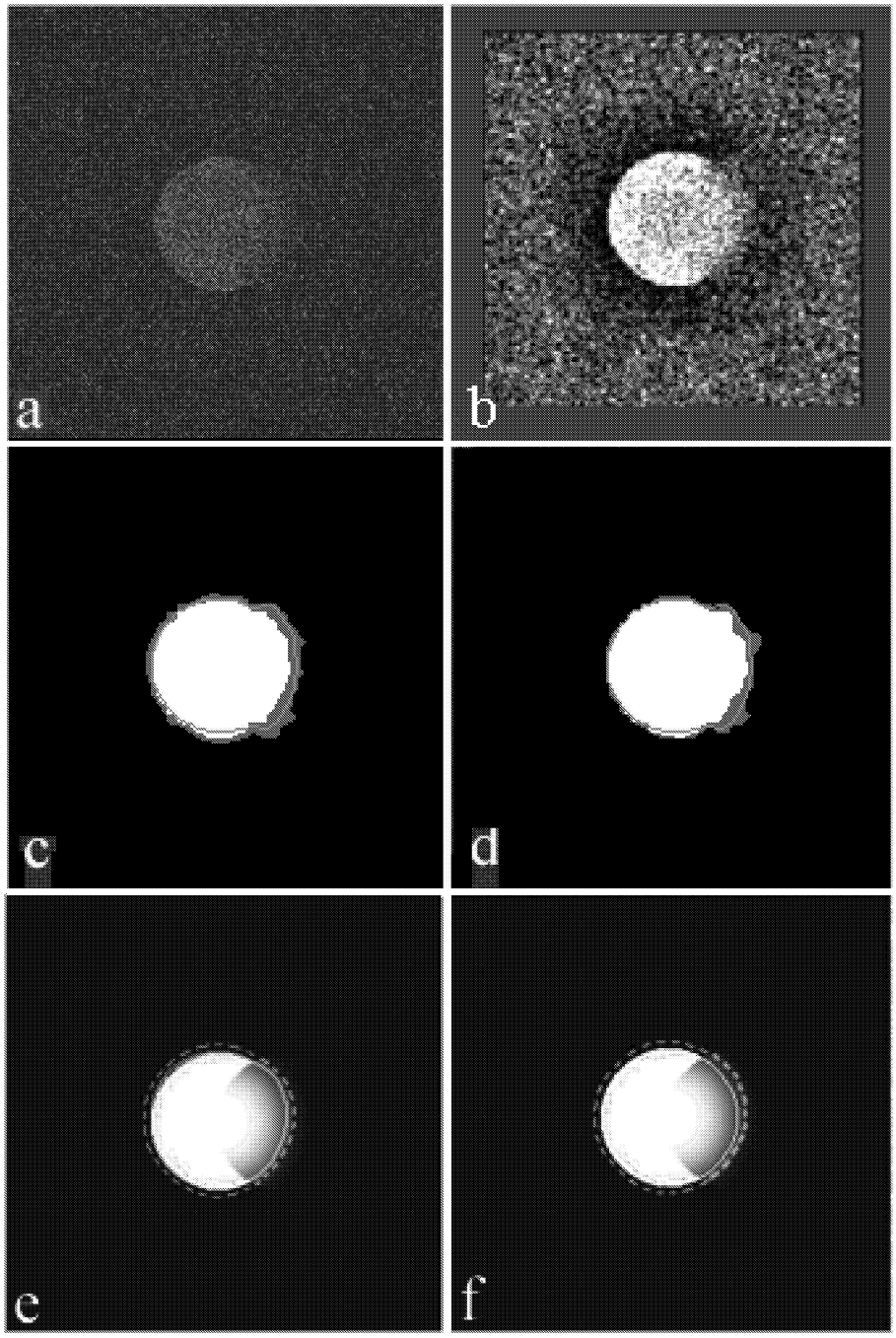

Fig. 1. a) A model of a low contrast lung nodule. Gaussian blurring with kernel of 10x10 pixels was used on the right side of circle margin to model inclination and invasion of nodule margin into the background. A noise was added to model a complex image background (lung tissues). On this image there is a Gaussian noise with standard deviation of s=16.

b) Processing of initial test image.

c) Initial and d) processed test images after segmentations SEGM1 (marked with white) and SEGM2 (marked with gray), which was accomplished by filtration of small details.

Gray line is the contour of the object outlined manually by a physician on the modeling circle with blurred margin.

e-f) Contours of SEGM3 for the initial and processed images were obtained for two levels: 0.75 (dropped line) and 0,5 (white line). These contours are added to the modeling circle (Fig.1b), displayed with correction of gray levels.

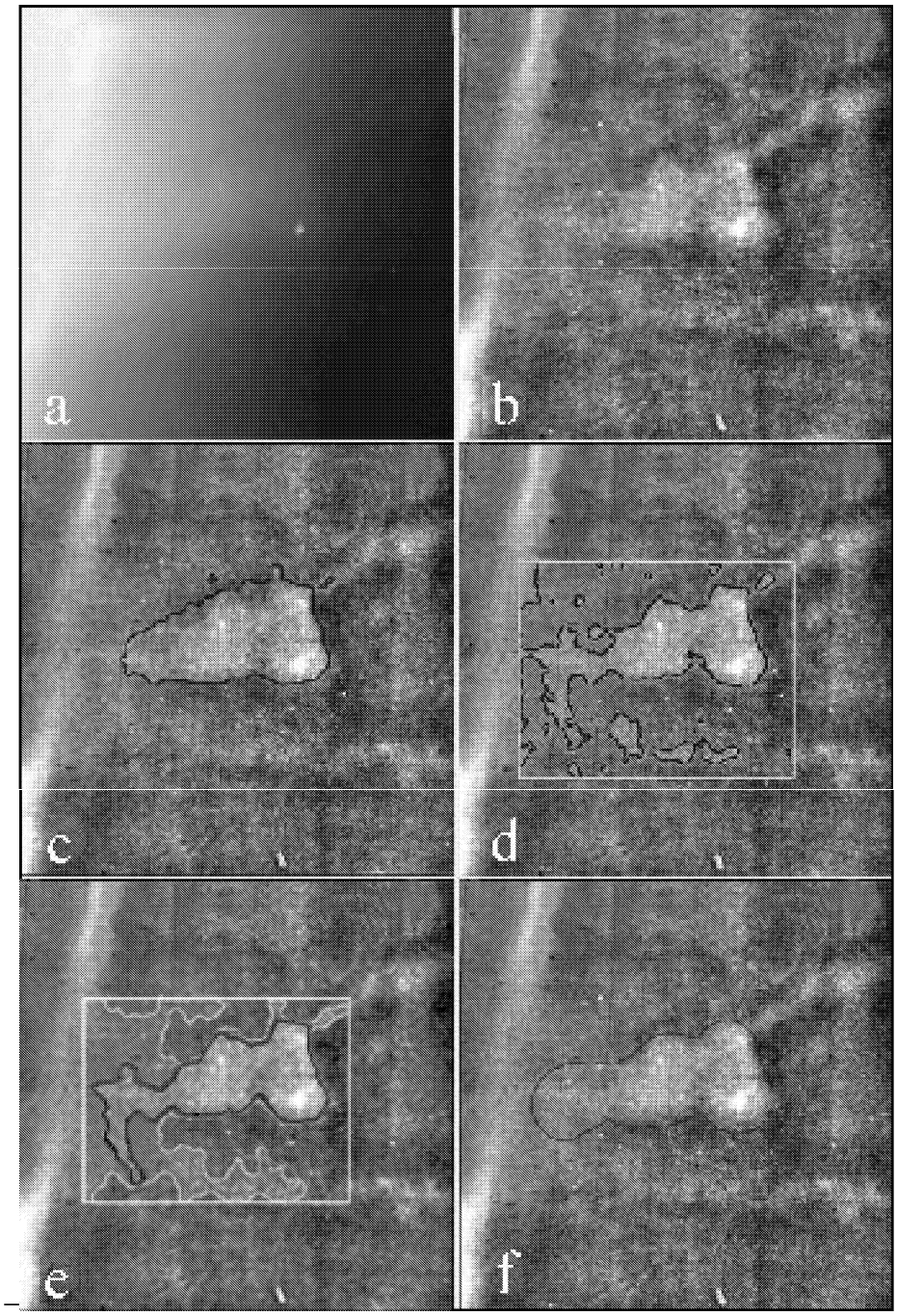

Fig.2. Tomogram 1. Comparison of results after SEGM1, SEGM2 and SEGM3.
a) Original tomogram. b) Tomogram after optimal filtering. c), d) Contours after the segmentation SEGM1 of the original (a) and processed (b) tomogram are added to the processed image. e) Contours after segmentation SEGM1 (black) and SEGM2 (gray) of the processed tomogram with filtering of small-size regions. f) Contours after segmentation SEGM3 of the processed tomogram.

the processed images were higher in comparison with those of the original image (see Fig. 3 b, d) because of numerous small-size details stressed by optimal filtering and extracted by segmentation. Size-based filtering [Choch88] helps to remove small-size regions from the segmented image. After segmentation SEGM2 and filtration of small details the misclassification rates for the processed test images are better in comparison with those of the initial test images, however, false alarm rates of SEGM2 are smaller for the initial test images (Fig. 3 e-f). In general, segmentation SEGM2 with following filtering of small-size details gives stable middle levels for both misclassification and false alarm rates in comparison with SEGM1. Our analysis shows that segmentation SEGM2

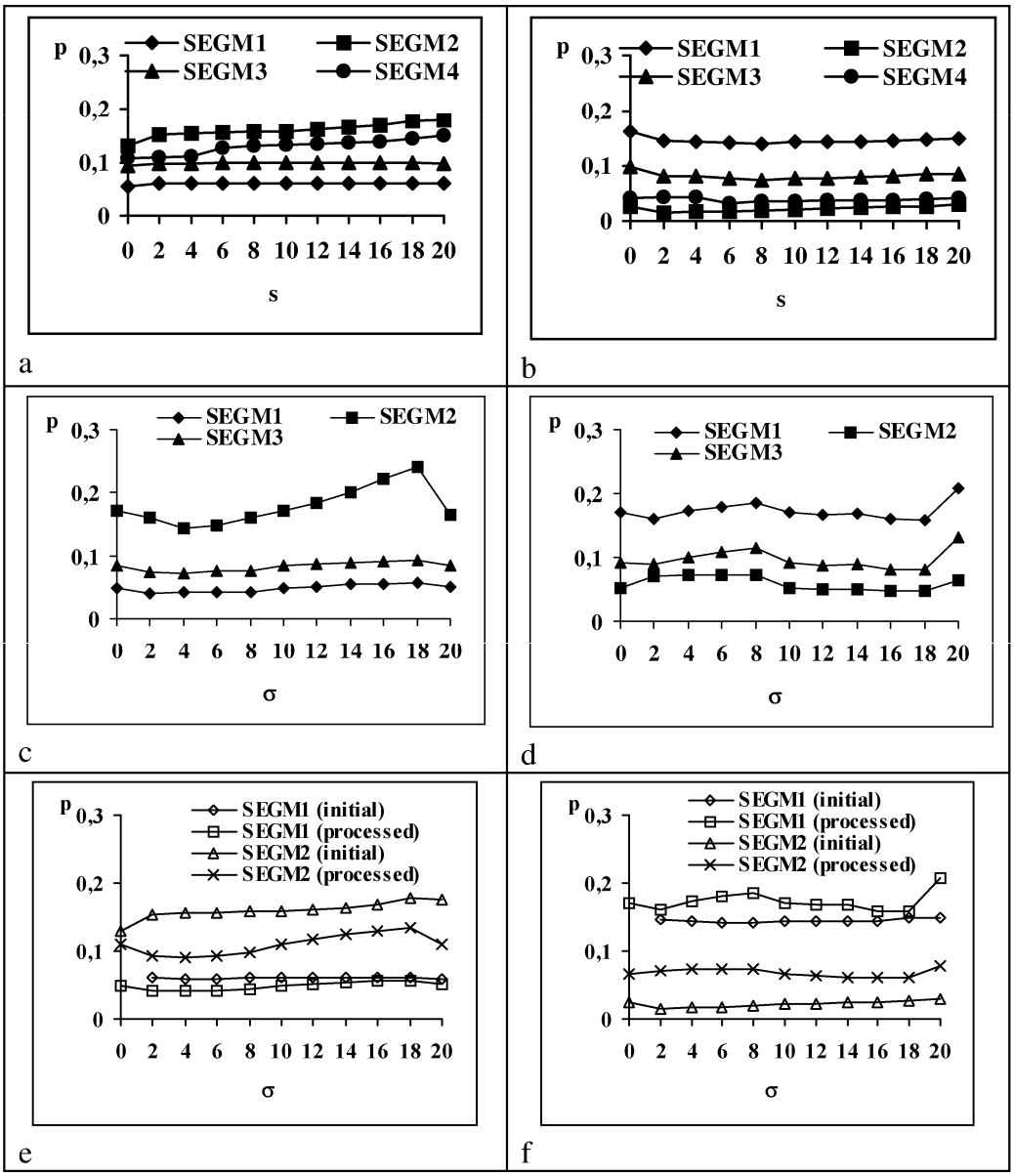

Fig 3. False alarm and misdetection rates for the segmentation of initial and processed test image corrupted by Gaussian noise with standard deviation σ. a) False alarm and b) misdetection rate for the segmentation of the initial test images; c) false alarm rate and d) misdetection rate for the segmentation of the processed test images; e) false alarm and misdetection rates after filtering of small details for the initial test images and f) processed test images

of the processed image outlines well the sharp part of margin and shows invasion of margins into the surrounding tissues.

SEGM3 On Fig. 1 e,f there are contours, obtained for two sizes of structuring elements for the initial and processed images respectively. Analysis of segmented images showed, that segmentation SEGM3 (0,75) doesn't match well the object region on the initial and processed images. SEGM3(0,5) gives better results and fits better to the region of object. Such segmentation is not sensitive to margin declination. Misdetection rates for SEGM3 are worse in comparison with those for SEGM1 and better than those for SEGM2, and for the false alarm rates there is on the contrary result (see Fig.3).

Proposed methods were compared with histogram based segmentation method proposed by Otsu [Otsu78] (see SEGM4 on Fig. 3). Segmentation was made in the region of interest localized by relevance function (See Ch. 2.1). False alarm rates for Otsu method are close to SEGM2: they are worse in comparison with those for SEGM1 and SEGM3 and better than those for SEGM2. Misdetection rates are worse in comparison with those for SEGM2 and better_than those for SEGM1 and SEGM3.

Comparison of the results, obtained by segmentation SEGM1, SEGM2 and SEGM3 of the original and processed lung tomogram is presented on Fig.2. On Fig. 2 c,d there are contours of regions matched by segmentation SEGM1 on the original and processed tomograms respectively. Fig. 2e shows the result of segmentation SEGM1 and SEGM2 of the processed tomogram after filtering of small-size details. SEGM3 of the processed tomogram is shown on Fig. 2f. The visual analysis shows that optimal filtering with following filtration of small-size regions allows to outline the object margins better and marks the shadows of vessels. Segmentation SEGM3 revealed well the object margin, too, but it has given more generalized region to the left of the nodule (see a low contrast shadow on Fig. 2b).

4. CONCLUSIONS

Series of methods have been developed for automatic detection and improved segmentation of low-contrast objects, situated on a complex background. A model-based structural approach to object detection and image segmentation has been developed and applied for automatic detecting and segmenting regions with solitary nodules on test images and lung tomograms. Robust estimation of model parameters has provided easy tuning and fitness of segmented region to the object.

Three types of segmentation algorithms have been proposed to improve matching of segmented region to the area of interest. Their comparison showed that they could help to outline the object region and to reveal specific features of object margins (in particular, outline shadows of converging vessels, areas with invasion of margins into surrounding tissues, etc). The optimal linear filtering was applied to emphasize manifestation of details on the object and on the object margin. Our experiments and comparisons showed that optimal filtering with following filtration of small-size details improves results of segmentation and gives more precise matching of the segmented region to the nodule.

Developed methods can be used for automatic or semi-automatic image screening. They could help realize automatic evaluation of some object features, such as edge profile acutance; edge sharpness; object perimeter, square, shape; dense variation, etc. It could support analysis and classification of images by an expert or with the use of machines.

ACKNOWLEDGMENTS

We'd like to thank Dr. P. Chochia for his help with filtering of small-size details, which was fulfilled on his image processing system IRBIS.

REFERENCES

[Aylwd97] Aylward,S, Pizer,S: Continuous Gaussian Mixture Modeling, Information Processing in Medical Imaging, *Lecture Notes in Computer Sciences,* Vol.1230, pp.176-189, 1997.

[Baret96] Barrett,H, Swindell,W: Radiological imaging *Theory of image formation, detection and processing. Academic press, San-Diego*, 1996.

[Belik94] Belikova,T, Yashunskaya,N, Kogan,E: Computer analysis for differential diagnosis of small pulmonary nodules: Int. Congress for lung cancer. Athens Greece, Monduzzi. Editore. Intern., pp.93-98, 1994.

[Belik96] Belikova,T, Yashunskaya,N, Kogan,E: Computer-Aided differential Diagnosis of Small solitary Pulmonary Nodules. *Computer and Biomedical Research*, Vol.29, No.1, pp.48-62, 1996.

[Breil99] Brejl,M, Sonka,M: Medical image segmentation: automated design of border detection criteria from examples, Journal of Electronic Imaging, No.1, pp.54-64, 1999.

[Chen97] Chen,C, Lee,G: On digital mammogram segmentation and microcalcification detection using multi-resolution wavelet analysis, *CVGIP: Graph. Models and Image Processing*, Vol.59, No.5, pp.348-364, 1997.

[Choch88] Chochia,P: Image enhancement using sliding histogram, *Computer Vision, Graphics, and image processing* Vol.44, pp.211-229, 1988.

[Palen00] Palenichka,R, Belikova,T, and Ivasenko,I: Robust extraction of diagnostic features of features of lesions from medical radiographic images, *Machine Graphics and Vision,* Vol.9, No.1-2, pp.473-496, 2000.

[Palen99a] Palenichka,R, Zinterhof,P, Ivasenko,I: Image Filtering and Segmentation Using Robust Structure-Adaptive Estimation of Intensity, Proc. of TELSIKS-99 Nis, Yugoslavia, pp.159-168, 1999.

[Petrs94] Petrosian,A *et al.* Computer-aided diagnosis in mammography: classification of mass and normal tissue by texture analysis, *Phys. med Biol.,* Vol.39, pp.2273-2288, 1994.

[Proc00a] Proceedings of 16th Symposium for Computer Applications in Radiology. PACS: Performance Improvement in Radiology. Houston, USA 1999*, J. of Digital Imaging* **12**, 2, 2000.

[Otsu78] Otsu,N A threshold selection method from grey-level histograms. IEEE Trans. Syst., Man, Cybern., vol SMC-8, pp 62-66, 1978

[Wei97] Wei,D, et al. False-positive reduction technique for detection of masses on digital mammograms: global and local multiresolution texture analysis. *Medical physics*, Vol.24, No.6, pp.903-914, 1997.